RESEARCH ARTICLE

Sinusoidal Organic Anion-Transporting Polypeptide 1B1/1B3 and Bile Canalicular Multidrug Resistance-Associated Protein 2 Play an Essential Role in the Hepatobiliary Disposition of a Synthetic Cyclic Dinucleotide (STING Agonist)

Philip Sandoval[1] · Bei-Ching Chuang[1] · John K. Fallon[2] · Philip C. Smith[2] · Swapan K. Chowdhury[3] · Robert J. Griffin[1] · Cindy Q. Xia[4] · Shinji Iwasaki[5] · Paresh P. Chothe[1]

Abstract
The liver is central to the elimination of many drugs from the body involving multiple processes and understanding of these processes is important to quantitively assess hepatic clearance of drugs. The synthetic STING (STimulator of INterferon Genes protein) agonist is a new class of drugs currently being evaluated in clinical trials as a potential anticancer therapy. In this study, we used ML00960317 (synthetic STING agonist) to investigate the hepatobiliary disposition of this novel molecular entity. A bile-duct cannulated (BDC) rat study indicated that biliary excretion is the major route of elimination for ML00960317 (84% of parent dose in bile). The human biliary clearance using *in vitro* sandwich cultured human hepatocyte model predicted significant biliary excretion of ML00960317 (biliary excretion index (BEI) of 47%). Moreover, the transport studies using transporter expressing cell lines, hepatocytes, and membrane vesicles indicated that ML00960317 is a robust substrate of OATP1B1, OATP1B3, and MRP2. Using relative expression factor approach, the combined contribution of OATP1B1 (fraction transported (f_t) = 0.62) and OATP1B3 (f_t = 0.31) was found to be 93% of the active uptake clearance of ML00960317 into the liver. Furthermore, OATP1B1 and OATP1B3-mediated uptake of ML00960317 was inhibited by rifampicin with IC_{50} of 6.5 and 2.3 μM, respectively indicating an *in vivo* DDI risk (R value of 1.5 and 2.5 for OATP1B1 and OATP1B3, respectively). These results highlighted an important role of OATP1B1, OATP1B3, and MRP2 in the hepatobiliary disposition of ML00960317. These pathways may act as rate-determining steps in the hepatic clearance of ML00960317 thus presenting clinical DDI risk.

Keywords cyclic dinucleotide · drug-drug interaction · hepatobiliary disposition · MRP2 · OATPs

✉ Paresh P. Chothe
pareshchothe@yahoo.com

1 Global Drug Metabolism and Pharmacokinetics, Takeda Development Center Americas, Inc. (TDCA), 95 Hayden Avenue, Lexington, Massachusetts 02421, USA

2 Division of Pharmacoengineering and Molecular Pharmaceutics, UNC Eshelman School of Pharmacy, University of North Carolina at Chapel Hill, Chapel Hill, North Carolina, USA

3 Present Address: Boston Pharmaceuticals, 55 Cambridge Parkway, Suite 400, Cambridge, Massachusetts 02142, USA

4 ReNAgade Therapeutics Management Co., 450 Kendall Street, Cambridge, Massachusetts 02142, USA

5 Drug Metabolism and Pharmacokinetics Research Laboratories, Takeda Pharmaceutical Company Limited, 26-1, Muraoka-Higashi 2-Chrome, Fujisawa, Kanagawa 251-8555, Japan

Springer

Introduction

A well-balanced immune system (innate and adaptive immunity) is critical to our body's defense mechanism to fight against infections and cancers. With growing understanding of the health benefits of a balanced immune system, immuno-oncology has shown tremendous potential in the development of promising treatments to fight against cancers by manipulating body's immune system (1). Among various immunotherapy possibilities, harnessing innate immunity has shown benefit in precise and personalized treatment of cancer patients. One such potent anti-cancer approach involves targeting the 2′3′-cyclic-GMP-AMP (cGAMP)- 1 Stimulator of Interferon Genes (STING) innate immunity pathway (2, 3). cGAMP is a cyclic dinucleotide (CDN) that functions as an immunotransmitter. It activates the STING pathway to release antitumor cytokines such as interferon-beta (IFN-β) which later triggers downstream adaptive immunity to elicit systemic antitumor effects (4). Considering this robust antitumoral immune response of cGAMP, there is a growing interest in developing synthetic dinucleotides (cGAMP analogs) as novel cancer therapeutics.

ML00960317 is a STING agonist with a synthetic CDN structure (Fig. 1), and it has shown potent antitumor activity in nonclinical tumor models by inducing robust innate and adaptive immune responses (5). Generally, endogenous cGAMP and its synthetic analogs such as ML00960317 have moderate-to-high molecular weight (> 400) and low permeability (Supplemental Table 6) and therefore, uptake transporters play an obligatory role in their pharmacological effects in target cells (6, 7). Mechanistic understanding of hepatic disposition of drugs is important in early drug discovery not only to identify rate-determining steps in their hepatic clearance but also to identify drug-drug interaction (DDI) liabilities. Based on the Extended Clearance Classification System (ECCS), the hepatic clearance of synthetic STING agonists (class 3B) is generally driven by hepatic uptake and bile canalicular efflux transporters (8). Hepatic uptake transporters such as organic anion-transporting polypeptides (OATPs) (9, 10), organic anion transporter (OAT) 2 (11), and organic cation transporter (OCT) 1 (12) and hepatic bile canalicular efflux transporters including p-glycoprotein (P-gp) (13), breast cancer resistance protein (BCRP) (14), and multidrug resistance-associated protein (MRP) 2 (15) are known to be involved in the hepatic uptake, clearance, and biliary excretion, respectively, of many drugs and hence liable for potential DDIs. OATPs are very well characterized with respect to their critical role in the hepatic clearance and associated DDI risk for substrate drugs including statins (9, 10), bosentan, simeprevir, and repaglinide (16). Besides DDIs, OATP1B1 polymorphism (in particular rs4149056, c.521T>C) has shown substantial impact on the PK of its substrate drugs. For example, the plasma level of atorvastatin, rosuvastatin, and repaglinide is increased by 1.5–3-fold in individuals with 512T>C polymorphism (17–20). Therefore, regulatory agencies (US FDA, EMA, and PMDA) require a systematic *in vitro* and *in vivo* evaluation of new chemical

Fig. 1 The chemical structure of ML00960317
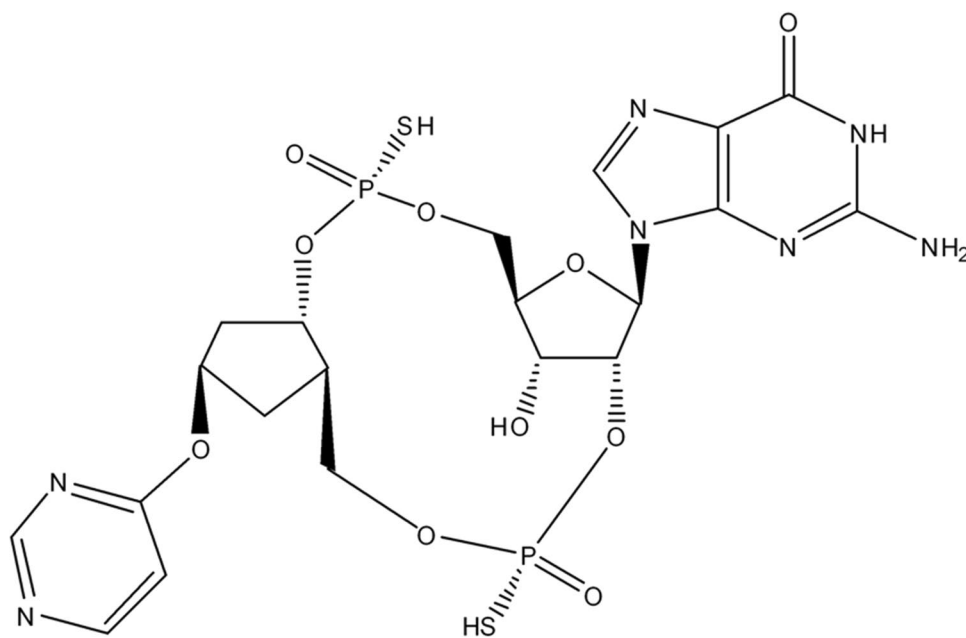
pKa= 0.67, 1.27 (acid)

entities (NCEs) as potential substrates and inhibitors of these drug transporters (FDA DDI Guidance 2020, EMA DDI Guidance 2013, and PMDA DDI Guidance 2018). Currently, there is limited literature describing the hepatobiliary disposition of synthetic CDNs (STING agonists) to identify the rate-determining steps in the hepatic clearance of these drugs and to predict DDI liabilities. Therefore, in the present study, we used ML00960317 (a synthetic CDN-based STING agonist) as a research tool (the structural analog of ML00960317 is currently under clinical development) to delineate the potential drug transporters involved in the hepatobiliary disposition of CDNs. The goals of this study were to — investigate elimination routes of ML00960317 using a bile-duct cannulated rat model, comprehensively characterize drug transporters involved in the hepatic uptake and biliary excretion of ML00960317, quantitatively determine OATP1B1 and OATP1B3 contributions to the hepatic uptake of ML00960317 using the relative expression factor (REF) approach, and predict *in vivo* DDI risk with OATP1B perpetrators.

Materials and Methods

Transporter-qualified cryopreserved human hepatocyte lots (8339 and 8350) were purchased from ThermoFisher Scientific (Waltham, MA, USA) (Supplemental Table 9). Williams' E medium, cryopreserved hepatocyte recovery medium, hepatocyte maintenance, and plating supplement pack were purchased from Thermo Fisher (Waltham, MA, USA). Atorvastatin, rifamycin SV, N-methyl quinidine, valspodar, Ko143, and benzbromarone were obtained from Sigma-Aldrich (St. Louis, MO, USA). [^{3}H]atorvastatin, [^{3}H]estradiol-17β-glucuronide, [^{3}H]estrone-3-sulfate, and [^{3}H]TCA were purchased from American Radiolabeled Chemicals Inc. (St. Louis, MO, USA). [^{3}H] Guanosine 3′,5′-cyclic phosphate (cGMP) was procured from Perkin Elmer (Waltham, MA, UA). ML00960317 was prepared and supplied by Takeda Pharmaceutical company. All organic solvents were of the highest quality and procured from Thermo Fisher (Waltham, MA, USA) and Sigma-Aldrich (St. Louis, MO, USA).

Pharmacokinetic Analysis of ML00960317 in Control and Bile-Duct Cannulated (BDC) Rats

The pharmacokinetic of ML00960317 in bile-duct cannulated and non-cannulated male Sprague-Dawley rats was conducted at the Takeda animal testing facility accredited by the Association for Assessment and Accreditation of Laboratory Animal Care (AAALAC). The experimental procedure was followed as per the Animal Welfare

Act and National Research Council (NRC) guidelines. Briefly, bile-duct cannulated ($n = 4$) and non-cannulated ($n = 3$) male Sprague-Dawley rats were administered ML00960317 as a single 1 mg per kg dose intravenously in sterile phosphate buffer saline through a jugular vein catheter. Plasma samples were collected at specified time points (from 0.0833 to 48 h). Bile (BDC rats only) and urine samples were collected from 0 to 8 h, 8–24 h, and 24–48 h postdose while feces samples were collected from 0 to 24 h and 24–48 h postdose. A total of 0.5 mL of bile fluid replacement solution (0.5% glucose/40 mM sodium taurochlorate/5 mM potassium chloride/0.9% sterile saline) was administered to each animal (BDC rats) through a return catheter into the duodenum once every hour from 1 to 8 h and 24 to 32 h postdose. All the samples were stored ≤ 70°C until LC-MS/MS analysis.

Measurement of Biliary Excretion of ML00960317 in Sandwich Cultured Human Hepatocytes (SCHH)

The biliary excretion of ML00960317 was measured using sandwich cultured human hepatocytes. The study was performed at Qualyst Transporter Solutions (a BIOIVT Company). Briefly, transporter-qualified cryopreserved human hepatocytes (Lot WWQ) were thawed in warm (37°C) water bath for 2 min. Cells were decanted into 45 mL of warm BioIVT proprietary Qual-GroTM Thaw Media. Following centrifugation (~100×g for 8 min), media was aspirated and cells were resuspended in QualGroTM Seeding Medium (~1 mL/million cells). Hepatocytes were suspended in QualGroTM Seeding Medium) at a density of 0.8–1.2 million viable cells/mL and seeded onto BioCoat® 24-well cell culture plates. Twenty-four hours later, cells were over-laid with QualGroTM Hepatocyte Culture Medium supplemented with extracellular matrix (ECM), Matrigel® (0.25 mg/mL). Cells were maintained in QualGroTM Hepatocyte Culture Medium until used in the study.

Uptake Studies of ML00960317 Using Hepatic Uptake Transporter- (OATP1B1, OATP1B3, OATP2B1, NTCP, OAT2) Overexpressing Cell Lines

The uptake studies in OATP1B1 and OATP1B3 cells were conducted in-house, whereas uptake studies using MDCKII-OATP2B1, MDCKII-NTCP, and MDCKII-OAT2 were performed at Optivia Biotechnology. In brief, HEK-OATP1B1, HEK-OATP1B3, and HEK-mock cells were grown on poly-D-Lysine precoated 48-well plates while MDCKII-NTCP, MDCKII-OAT2, and MDCKII-mock cells

were grown on permeable support in a 96-well plate. Cells were washed twice with prewarmed Hank's balanced salt solution (HBSS). HBSS buffer containing ML00960317 in the absence or presence of transporter inhibitor was added to cells. For positive controls, OATP1B1 and OATP1B3, OATP2B1, NTCP, and OAT2 expressing cells were incubated with [3H]estradiol-17β-glucuronide (0.06 µM), [3H] estrone-3-sulfate (0.5 µM), [3H]TCA (2 µM), and [3H]cyclic guanosine monophosphate (cGMP) (2 µM), respectively. After 5-min incubation, the dosing solution was aspirated from the cells and the uptake was stopped by washing the cells 3 times with ice-cold HBSS buffer. Cells were then lysed with 200 µL of Triton™ X-100 (Sigma-Aldrich Company LLC [St. Louis, MO, USA]) (0.5%, volume-to-volume ratio [v:v]) in phosphate-buffered saline (PBS). Cell lysates were placed into a 96-well Wallac Isoplate™ (PerkinElmer Life Sciences [Waltham, MA, USA]) and mixed with 150 to 200 µL of Ultima-Flo™ M liquid scintillation cocktail (PerkinElmer Life Sciences [Waltham, MA, USA]). The radioactivity in each sample was measured with a 2450 MicroBeta2® TriLux microplate scintillation and luminescence counter (PerkinElmer Life Sciences [Waltham, MA, USA]). The cellular accumulation of ML00960317 was quantified by LC-MS/MS.

Uptake Analysis of ML00960317 in Plated Human Hepatocytes

Cryopreserved human hepatocytes were thawed using cryopreserved hepatocyte recovery medium (CHRM) (Life Technologies Corporation) and centrifuged at 100×g for 10 min at room temperature. The cell pellets were suspended in William's Medium E (WME) (Invitrogen [Carlsbad, CA, USA]) containing 0.1-mM nonessential amino acids, 2-mM L-glutamine, 4.5-g/L glucose, 10% fetal bovine serum (FBS), insulin-transferrin-selenium (1×) (Gibco), 0.1-µM dexamethasone, and 100-unit/mL penicillin/streptomycin. The hepatocytes were seeded at a density of 0.15 to 0.2 million cells per well onto 48-well plates precoated with Collagen I (Corning Life Sciences) (Corning, NY, USA). The hepatocytes were allowed to attach at 37°C for approximately 1 h with 95% air and 5% CO$_2$, and the medium was replaced by WME containing 0.1-mM nonessential amino acids, 2-mM L-glutamine, 4.5-g/L glucose, insulin-transferrin-selenium (1×), 0.1-µM dexamethasone, and 100-unit/mL penicillin/streptomycin. The hepatocytes were further incubated at 37°C for an additional 3 to 4 h before use in the assay.

To initiate the uptake assay, first hepatocytes were equilibrated with KHB buffer for 10 min at 37°C. Later, hepatocytes were incubated with ML00960317 at 37°C and 4°C to measure the total uptake and passive diffusion, respectively. To assess the role of hepatic OATPs, hepatocytes were preincubated with 20 µM rifamycin SV for 15 min and then co-incubated with rifamycin SV (20 µM) and ML00960317 for 5 min at 37°C. As a positive control, the uptake of [3H] atorvastatin was measured at 37°C in the absence and presence of rifamycin SV (20 µM) and, 4°C. At the end of uptake period, hepatocytes were washed 3 times with ice-cold KHB buffer. The cells were lysed with Triton™ X-100 (Sigma-Aldrich Company LLC [St Louis, MO, USA]) (0.5%, v:v) in phosphate-buffered saline (PBS). The samples were analyzed for the quantification of ML00960317 by LC/MS/MS. The radioactive samples ([3H]atorvastatin) were mixed with Ultima-Flo™ M liquid scintillation cocktail (PerkinElmer Life Sciences [Waltham, MA, USA]) and the radioactivity in the samples was measured with a 2450 MicroBeta2® TriLux microplate scintillation and luminescence counter (PerkinElmer Life Sciences [Waltham, MA, USA]). The total protein concentration in cell lysates was quantified using the Pierce™ bicinchoninic acid (BCA) protein assay (Thermo Fisher Scientific, Inc. [Rockford, IL, USA]), with bovine serum albumin (BSA) as the reference standard. The cellular accumulation of ML00960317 and [3H]atorvastatin was normalized to the total protein concentration. All experiments were conducted in triplicate ($n = 3$).

Transport Studies of ML00960317 with Bile-Canalicular Efflux Transporters

The transport of ML00960317 into membrane vesicles was analyzed using inside-out membrane vesicles prepared from HEK293 cells individually overexpressing human BCRP, MDR1, and MRP2 (SOLVO Biotechnology, Hungary). The membrane vesicles prepared using cells without transporter expression were used as a negative control. Briefly, transporter overexpressing and control membrane vesicles (50 µg) were incubated with ML00960317 at 0.18, 1.83, and 9.15 µM in the presence of ATP and AMP for 10 min. The reactions were terminated by the addition of ice-cold washing buffer and immediate filtration via glass fiber filters mounted to a 96-well plate (filter plate). Subsequently, the filters were washed five times with ice-cold washing buffer and dried. The filters were finally washed with methanol:water (2:1) and the amount of ML00960317 accumulated inside the vesicles was quantified by LC-MS/MS.

Permeability Assessment of ML00960317 Using Caco-2 Cells

Caco-2 cells were seeded onto 24-Transwells plate (0.33 cm^2/well, 0.4 µm pore size, Costar) at an initial density of 1×10^5 cells/well and incubated at 37°C in an atmosphere

Table I Disposition of an Intravenous Bolus Dose of ML00960317 in Control and Bile-Duct Cannulated Male Sprague-Dawley Rats

Parameters	Control rats ($n = 3$)	BDC rats ($n = 4$)
AUC_{inf} (hr*ng/ml)	313 ± 20	291 ± 148
C_{max} (ng/ml)	1110 ± 75.5	941 ± 379
$T_{1/2}$ (hr)	0.27 ± 0.1	0.37 ± 0.15
CL (L/h/kg)	3.21 ± 0.2	3.96 ± 1.4
Vss (L/Kg)	0.42 ± 0.06	0.66 ± 0.11
% Dose in bile	ND	84.3 ± 9.25
Biliary clearance (L/h/Kg)	ND	3.14 ± 1.28
% Dose in urine	4.53 ± 3.06	10.1 ± 5.36
Renal clearance (L/h/Kg)	0.15 ± 0.10	0.14 ± 0.12
% Dose in feces	41.7 ± 15	0.20 ± 0.28

ND, not determined. Both the control ($n = 3$) and BDC ($n = 4$) male Sprague-Dawley rats were administered ML00960317 as a single 1 mg/kg dose intravenously in sterile phosphate buffer saline through a jugular vein catheter

of 5% CO_2 in air and 90% humidity. The cells were cultured for 21–25 days to differentiate them into enterocytes-like cells. The transepithelial electrical resistance (TEER) was measured to ensure tight junction formation and cells with TEER value more than 250 ohms $\times$ cm^2 were used in the study. On the day of transport study, cells were washed

and then equilibrated with warm HBSS buffer for 60 min. ML00960317 at a concentration of 5 µM (containing 50 µM Lucifer Yellow (zero permeability marker)) was added in 24 Transwell cell plate (apical 210 µL and basal 1000 µL) and buffer was added in the receiver side (apical 200 µL and basal 1000 µL). At the end of incubation, samples from receiver side were aliquoted (120 µL) and mixed with acetonitrile (with 0.1% formic acid) containing 100 nM carbutamide (internal standard). Samples were analyzed for quantification of ML00960317 by LC-MS/MS.

Quantification of Uptake Transporter Proteins in Human Hepatocytes and HEK-293 Cells Overexpressing OATP1B1 and OATP1B3 by Quantitative Targeted Proteomics

The membrane protein abundance of uptake transporters in human hepatocytes lot 8339 and lot 8350, shown in Tables I, II, III, is adopted from our previous study (21). Additionally, we quantified membrane protein expression of reduced-folate carrier (*SLC19A1*) in human hepatocytes lot 8339 and 8350. The membrane protein expression of OATP1B1

Table II Biliary Clearance of ML00960317 in SCHH

Compound	Target concentration (μM)	Dose concentration (μM)	Total accumulation (pmol/mg)	Cellular accumulation (pmol/mg)	Bile accumulation (pmol/mg)	BEI (%)	Biliary clearance (ml/min/kg)
ML00960317	2	2.02	5.97 ± 0.59	3.19 ± 0.5	2.78 ± 0.78	46.6 ± 14	0.20 ± 0.06
d8-TCA	5	4.47	1680 ± 100	997 ± 39	679 ± 110	40.5 ± 7	22.5 ± 3.6
d8-TCA*	5	2.02	752 ± 45	446 ± 17	306 ± 48	40.7 ± 6.8	22.7 ± 3.6
Digoxin	10	10.4	416 ± 25	308 ± 38	108 ± 45	25.9 ± 11	1.53 ± 0.64
Digoxin*	10	2.02	80 ± 4.8	59.2 ± 7.3	20.8 ± 8.7	26.0 ± 11	1.54 ± 0.64

*Dose concentraton of d8-TCA and digoxin is normalized to compare their total accumulation with ML00960317 at 2.02 µM

Table III Protein Abundance of Liver Uptake Transporters in Human Hepatocytes, and OATP1B1 and OATP1B3 in OATP1B1 and OATP1B3 Overexpressing HEK Cells

Protein	Proteotypic peptide sequence	pmol/mg membrane protein ($n = 2$) (mean $\pm$ SD)			
		Hepatocyte lot 8339	Hepatocyte lot 8350	HEK-OATP1B1	HEK-OATP1B3
OATP1B1	NVTGFFQSFK	8.51 ± 0.69*	8.59 ± 0.01*	84.67 ± 0.47	ND
OATP1B3	IYNSVFFGR	1.62 ± 0.63*	1.5 ± 0.08*	ND	41.09 ± 0.08
OATP2B1	YYNNDLLR	1.4 ± 1.9*	2.74 ± 0.7*	ND	ND
NTCP	GIYDGDLK	0.41 ± 0.05*	2.11 ± 0.56*	ND	ND
OCT1	LSPSFADLFR	3.25 ± 0.19*	2.32 ± 0.13*	ND	ND
OAT2	NVALLALPR	1.04 ± 0.25*	1.80 ± 0.17*	ND	ND
RFC[#]	QVPVEPGPDPELR	ND	ND	1.39 ± 0.65	1.08 ± 1.53

ND, not detected (*LLOQ*, lower limit of quantification = 0.1 pmol/mg protein). *Data is adopted from our recent study (21). [#]Reduced-folate carrier

and OATP1B3 was also quantified in HEK-293 cells over-expressing these transporters. All the measurements were done by quantitative targeted proteomics approach using nanoLC-MS/MS at the laboratory of Dr. Philip Smith at the University of North Carolina, Chapel Hill. The procedure of membrane protein extraction, trypsin digestion, and bioanalysis by LC-MS/MS was used as described previously (22, 23). The same quantification protocol has previously been used to quantify transporter-mediated clearance using REF approach (24). The details of surrogate peptides of transporters and the multiple reaction monitoring (MRM) used in this analysis are provided in the Supplemental Table 8.

Contribution of OATP1B1 and OATP1B3 to the Hepatic Uptake of ML00960317 Using REF Approach

The contribution of OATP1B1 and OATP1B3 to the hepatic uptake of ML00960317 was estimated using REF approach (25). The absolute protein abundance data of OATP1B1 and OATP1B3 in recombinant HEK-293 cells and human hepatocytes was used to derive the REFs for OATP1B1 and OATP1B3 using Eqs. 1 and 2, respectively.

$$REF_{1B1} = \frac{PE_{1B1,Hep}}{PE_{1B1,HEK-1B1}} \tag{1}$$

$$REF_{1B3} = \frac{PE_{1B3,Hep}}{PE_{1B3,HEK-1B3}} \tag{2}$$

Where, PE is the protein abundance of OATP1B1 and OATP1B3 in pmol/mg protein in hepatocytes and recombinant HEK-293 cells.

The active uptake clearance of ML00960317 mediated by OATP1B1 ($CL_{active,1B1,Hep}$) and OATP1B3 ($CL_{active,1B3,Hep}$) was estimated (REF-based scaling) using the following equations:

$$CL_{active,1B1,Hep} = CL_{active,HEK-1B1} * REF_{1B1} \tag{3}$$

$$CL_{active,1B3,Hep} = CL_{active,HEK-1B3} * REF_{1B3} \tag{4}$$

Data Analysis

The uptake data with error bars represent mean ± standard deviation (SD). The transport data obtained using cell lines and membrane vesicles was analyzed by Student's t test while the uptake data in human hepatocytes was analyzed by one-way analysis of variance (ANOVA) followed by Dunnett's

test among multiple groups with Prism 8.1.0 (GraphPad Software) to determine the statistical significance. The data were considered statistically significant when $P \leq 0.05$.

The active uptake kinetic parameters (K_m and V_{max}) were determined by using Michaelis Mentalis equation in Graph-Pad Prism 8.1.0 software (Graphpad Corp, La Jolla, CA, USA) as described in the equation below:

$$V = \frac{V_{max} \times S}{K_m + S} \tag{5}$$

Where, V is the uptake rate, V_{max} is the maximum transport velocity, K_m is the affinity of a substrate, and S is the substrate concentration.

In the vesicular transport substrate assay, the ATP-dependent transport of ML00960317 as well as the ATP-dependent fold accumulation in the transporter-containing vesicles was determined using the following equations:

$$ATP_{dependent\ transport} = n_{ATP} - n_{AMP} \tag{6}$$

$$Fold\ accumulation = \frac{n_{ATP}}{n_{AMP}} \tag{7}$$

Where, n_{ATP} is the amount of ML00960317 (pmol/mg) in the presence of 4 mM ATP and n_{AMP} is the amount of ML00960317 (pmol/mg) in the presence of 4 mM AMP transported into vesicles.

The biliary excretion index (BEI) and *in vitro* intrinsic Cl_{bile} (ml/min/kg) were determined in SCHH using the following equations (26):

$$BEI = \frac{\left(Accumulation_{cells+bile} - Accumulation_{cells}\right)}{Accumulation_{cells+bile}} \times 100 \tag{8}$$

$$Intrinsic\ CL_{bile} = \frac{\left(Accumulation_{cells+bile} - Accumulation_{cells}\right)}{AUC_{medium}} \tag{9}$$

where AUC_{medium} is the product of the incubation time and the medium concentration. The *in vitro* intrinsic CL_{bile} (ml/min/mg protein) was scaled using physiological scaling factors as follow: 1.5×10^6 cells per mg protein, 107×10^6 hepatocytes per gram human liver tissue (27) and 25.7 g of liver tissue per kilogram of body weight (28).

The *in vivo* CL_{bile} of ML00960317, d8-TCA, and digoxin was predicted using the following equation based on the well-stirred model of hepatic disposition:

$$Predicted\ CL_{bile} = \frac{Q_p \times fu,_p \times intrinsic\ CL_{bilie}}{Q_p + fu,_p \times intrinsic\ CL_{bile}} \tag{10}$$

Where Q_p and $fu,_p$ are the hepatic plasma flow rate (750 ml/min) (29) and plasma unbound fraction, respectively.

To predict the potential for ML00960317 to be a victim of DDI with OATP1B1 and OATP1B3 perpetrators such as rifampicin, the following equation was used to calculate the R value based on the FDA DDI Guidance 2020:

$$R = 1 + \frac{\left(f_{u,p} \times I_{in,max}\right)}{IC_{50}} \qquad (11)$$

Where, $f_{u,p}$ is the unbound fraction in plasma, IC_{50} is the half-maximal inhibitory concentration, and $I_{in,max}$ is the estimated maximum plasma concentration at the inlet to the liver of rifampicin.

$I_{in,max}$ is calculated using the following equation:

$$I_{in,max} = I_{max} + \left(F_a \times F_g \times K_a \times Dose\right)/Q_h/R_b \qquad (12)$$

Where, F_a is the fraction absorbed, F_g is the intestinal availability, K_a is the absorption rate constant, and R_B is the blood-to-plasma concentration ratio of rifampicin. Q_h is the hepatic blood flow rate (1500 mL/min). The input parameters of rifampicin used for the R value calculations are shown in Supplemental Table 7.

Results

Disposition of ML00960317 in Bile-Duct Cannulated (BDC) Rats

Pharmacokinetic (PK) study of ML00960317 was conducted in BDC rats and non-cannulated rats. The PK profile of ML00960317 is summarized in Table I. Overall, the PK profile of ML00960317 was comparable between BDC and non-canulated rats. The total CL of ML00960317 was found to be high (3.96 L/h/kg) whereas volume of distribution at steady state (Vss) was low (0.66 L/kg). The total amount of ML00960317 excreted into urine up to 48 h was 14,620 ng (4.42% of dose) and 32,011 ng (10.1% of dose) (per animal) in non-canulated and BDC rats, respectively, while the total amount excreted into feces up to 48 h was 138,459.7 ng (41.7% of dose) and 594.35 ng (0.2% of dose) (per animal) in non-canulated and BDC rats, respectively. The total amount of ML00960317 excreted into bile up to 48 h was 276,676 ng (84.3% of dose) in BDC rats. The mean biliary and renal clearance of ML00960317 were 3.14 and 0.14 L/h/kg, respectively, in BDC rats. The biliary and renal clearances accounted for 79% and 3.7% of total plasma clearance of ML00960317, respectively.

Measurement of Biliary Excretion of ML00960317 in SCHH

The hepatobiliary disposition of ML00960317 was evaluated in SCHH at 37°C at 2 μM for 20 min. d_8-TCA and digoxin were assessed in parallel as model drugs for significant and weak biliary clearance, respectively. The biliary excretion index (BEI) and biliary clearance values for d_8-TCA and digoxin were consistent with the literature data (30). These results demonstrated that the SCHH model has a functional bile canalicular network capable of supporting hepatic drug uptake and biliary efflux function.

The total accumulation (hepatocytes + bile), cellular accumulation (hepatocytes), and bile accumulation for ML00960317 in SCHH are shown in Table II. The total accumulation of ML00960317 was only 0.8% of the total accumulation of d_8-TCA, and 7.5% of the total accumulation of digoxin (after dose normalization). The BEI of ML00960317 was 46.6 ± 14% and it was similar to that observed for d_8-TCA (40.7 ± 6.8%), a model bile acid, with a high biliary efflux potential. BEI is a measure of biliary efflux potential describing the movement of a compound from inside the hepatocyte to the bile pockets. We subsequently determined apparent biliary clearance of ML00960317 which is more appropriate parameter for comparison to *in vivo* biliary excretion. Following a 20-min exposure, the biliary clearance of ML00960317 was 0.204 ± 0.057 mL/min/kg which was 111-fold lower than the biliary clearance of d_8-TCA (22.7 ± 3.6 mL/min/kg) and approximately 13% of the biliary clearance of digoxin in SCHH.

Substrate Analysis of ML00960317 for Major Hepatic Uptake Transporters (OATP1B1, OAP1B3, OATP2B1, NTCP, and OAT2)

The substrate potential of ML00960317 for major hepatic uptake transporters was investigated using OATP1B1, OATP1B3, OATP2B1, NTCP, and OAT2 overexpressed cell lines. The uptake of ML00960317 was measured at 1 μM for 5 min in both OATP1B1, OATP1B3, and HEK-mock cells. The accumulation of ML00960317 was found to be 14.5-fold and 7.3-fold higher in OATP1B1 and OATP1B3 cells, respectively, in comparison to HEK-mock cells indicating ML00960317 as a substrate of OATP1B1 and OATP1B3. Furthermore, the uptake of ML00960317 was significantly inhibited in the presence of an OATP1B1 and OATP1B3 inhibitor, rifamycin SV (20 μM) (Fig. 2a, c). ML00960317 was not accumulated significantly in OATP2B1, NTCP, and OAT2 expressing cells compared to MDCKII-mock cells (uptake ratio (transporter expressing cells/MDCKII-mock cells) < 2) (Fig. 2e, g, i). The positive control probe substrates, [³H]estradiol-17β-glucuronide (OATP1B1 and OATP1B3), [³H]estrone-3-sulfate, [³H]taurocholate, and [³H]cGMP showed significant uptake in the respective transporter cell lines indicating optimal transporter function (Fig. 2b, d, f, h, j).

Analysis of ML00960317 Uptake in PHH

To further support the role of OATP1B1 and OATP1B3 in the hepatic uptake of ML00960317, the uptake of this compound was analyzed in the absence and presence of 20 μM rifamycin SV (OATP inhibitor) at 37°C and at 4°C in plated human hepatocyte lots 8339 and 8350. The uptake of ML00960317 was found to be temperature dependent in both the lots. The total uptake of ML00960317 was significantly inhibited by rifamycin SV in both 8339 and 8350 lots (> 90%) (Fig. 3).

Characterization of ML00960317 Uptake in OATP1B1 and OATP1B3-Expressing HEK cells

Since the uptake of ML00960317 was only observed in HEK-OATP1B1 and HEK-OATP1B3 cells, we further characterized its uptake in these cell lines. First, we measured the time-dependent uptake of ML00960317 at 0.1, 1, and 10 μM in both OATP1B1 and OATP1B3 cells. The uptake was found to be linear up to 5 min in both OATP1B1 and OATP1B3 cells (Supplemental Fig. 1 and Supplemental Tables 1 and 2). The uptake ratio (OATP1B1 or OATP1B3/HEK-mock) of ML00960317 was ranged between 3 and 29.5-fold in OATP1B1 cells while between 2.3 and 16.36-fold in OATP1B3 cells indicating significant active uptake via OATP1B1 and OATP1B3 transporters (Supplemental Tables 1 and 2). Later, the uptake of ML00960317 was analyzed at different concentrations to determine the uptake kinetic parameters such as affinity (K_m) and maximum velocity (V_{max}) in both OATP1B1 and OATP1B3 cells. The kinetic analyses yielded K_m values of 12.9 and 19.3 μM and V_{max} values of 76 and 152.2 pmol/min/mg protein for OATP1B1 and OATP1B3, respectively (Fig. 4).

Transport of ML00960317 in MDR1, BCRP, and MRP2-Expressing Membrane Vesicles

The substrate potential of ML00960317 for bile canalicular efflux transporters, MDR1, BCRP, and MRP2 was tested in membrane vesicles expressing these transporters. The accumulation of ML00960317 in the presence of ATP and AMP (ATP-dependent fold accumulation was < 2) was similar in both MDR1 (Fig. 5a and Supplemental Table 3) and BCRP (Fig. 5b and Supplemental Table 4) vesicles, indicating no active accumulation, whereas the accumulation of ML00960317 was significantly higher in the presence of ATP compared to AMP (3.05 to 13.47-fold) in MRP2 vesicles, indicating active transport (Fig. 5c and Supplemental Table 5). In the follow-up inhibition assay, transport of ML00960317 was examined in the absence and presence of

MRP2 inhibitor, benzbromarone. The ATP-dependent accumulation of ML00960317 in the presence of benzbromarone was decreased from 7.7-fold to 1.3-fold (Supplemental Table 5), confirming ML00960317 as a substrate of MRP2. The positive control probe substrates, N-methyl quinidine (P-gp), estrone-3-sulfate (BCRP), and estradiol-17β glucuronide (MRP2) were run in parallel in the absence and presence of a reference inhibitor (valspodar for P-gp, Ko143 for BCRP, and benzbromarone for MRP2) and data confirmed the function of MDR1, BCRP, and MRP2 in the applied vesicles (Supplemental Tables 3–5).

Evaluation of OATP1B1 and OATP1B3 Contribution to the Hepatic Uptake of ML00960317 Using REF Approach

The transporter cell line and hepatocyte uptake data indicated that OATP1B1 and OATP1B3 are the major transporters involved in the hepatic uptake of ML00960317. Therefore, we quantitatively determined the contribution of these transporters to the active uptake clearance of ML00960317 using REF approach. First, REFs for OATP1B1 and OATP1B3 were calculated using absolute protein abundance of these transporters in human hepatocytes and HEK-OATP1B1 and HEK-OATP1B3 cell lines as described in experimental section. Subsequently, OATP1B1- and OATP1B3-mediated hepatic uptake clearances were estimated using REF-based scaling. The active uptake clearance of ML00960317 in human hepatocyte lots 8339 and 8350 was used to quantitatively describe the contribution of OATP1B1 and OATP1B3. Overall, both transporters contributed to ~91% and ~93% of active uptake of ML00960317 in lot 8339 and lot 8350, respectively. In terms of individual contribution, OATP1B1 contributed to 60% and 62% of active uptake in lot 8339 and lot 8350, respectively while OATP1B3 contributed to 31% of active uptake of ML00960317 in both the lots (Table IV). We also evaluated the contribution of OATP1B1 and OAP1B3 to the hepatic uptake of atorvastatin as positive control. Data indicated that total contribution of OATP1B1 and OATP1B3 to the active uptake clearance of atorvastatin was 85% and 61% in lot 8339 and lot 8350, respectively. OATP1B1 contributed to 52% and 38% of active uptake while OATP1B3 contributed to 33% and 23% of active uptake of atorvastatin in lot 8339 and lot 8350, respectively (Table IV).

Inhibition of OATP1B1- and OATP1B3-mediated ML00960317 uptake by Rifampicin and Prediction of Victim DDI Risk

To understand the liability of ML00960317 for victim DDI with an OATP1B perpetrator, the effect of rifampicin, a

Table IV Fractional Contribution of OATP1B1 and OATP1B3 to the Observed Active Clerance of ML00960317 and Atorvastatin Using Relative Expression Factor (REF) Approach

Compound	$Active_{Hep}$ (µL/min/mg)		CL (µL/min/mg)		REF-based scaling (µL/min/mg)				f_t (Lot 8339)		f_t (Lot 8350)		f_t (1B1 + 1B3)	
					Lot 8339		Lot 8350							
	Lot 8339	Lot 8350	1B1	1B3	1B1	1B3	1B1	1B3	1B1	1B3	1B1	1B3	Lot 8339	Lot 8350
ML00960317	0.99	0.96	5.9	7.9	0.59	0.31	0.60	0.30	59.7	31.4	62.0	31.0	91.1	93.0
Atorvastatin	13.1	18.2	67.8	109.2	6.82	4.30	6.89	4.14	52.2	33.0	37.9	22.8	85.2	60.8

clinical OATP1B inhibitor, on OATP1B1 and OATP1B3-mediated ML00960317 uptake was investigated. OATP1B1 and OATP1B3 overexpressing HEK cells were pre-incubated with rifampicin at different concentrations between 0.4 and 100 µM for 30 min and then the uptake of ML00960317 was measured in the presence of rifampicin in the same concentration range. Rifampicin dose-dependently inhibited OATP1B1 and OATP1B3-mediated ML00960317 uptake with an IC_{50} values of 6.5 and 2.3 µM, respectively (Fig. 6). To predict *in vivo* DDI risk, the static (model) equation (Eqs. 11 and 12) was used to estimate the R values based on US FDA DDI guidance (FDA DDI Guidance 2020). The calculated R values for OATP1B1 and OATP1B3 were 1.5 and 2.5 (> 1.1, the cutoff) indicating potential DDI risk *in vivo*.

Discussion

The STING pathway has shown a great promise in treating cancers and as such, there is growing interest in developing STING agonist analogs as a robust immunotherapy approach. In the present study, we have comprehensively characterized transporter pathways involved in the hepatobiliary disposition of the synthetic STING CDN agonist, ML00960317. We used ML00960317 as a tool CDN analog to gain mechanistic insights into hepatic disposition of this class of STING agonist analogs. ML00960317 has a molecular weight > 400 and it is anionic at physiologic pH (7.4) and therefore, it appears to have low permeability as indicated in Caco-2 cells (Supplemental Table 6). Typically, such compounds belong to the class 3B in the ECCS and according to this framework, the hepatic clearance of such compounds is determined by their hepatic uptake via transporters such as OATPs.

First, PK of ML00960317 was conducted in BDC rats to identify elimination pathways. Overall, the PK data indicated high CL and short terminal half-life of ML00960317 in rats. Interestingly, plasma CL, half-life and volume of distribution of ML00960317 was similar between BDC and non-cannulated rats suggesting no contribution of enterohepatic circulation to the systemic exposure of ML00960317. Furthermore, fecal elimination was dramatically reduced almost

to zero by bile duct cannulation suggesting that biliary CL of parent drug is the major clearance mechanism (recovery of 89% of the dose as parent drug). We also found that the biliary excretion of the parent drug in BDC rats was greater than the fecal excretion in non-cannulated rats (~84 *versus* 42%) suggesting that ML00960317 may not be stable in or has poor extraction from fecal homogenates. Further studies are needed to explain the role of intestinal microbiome in the degradation of ML00960317. The renal and biliary clearances accounted for 3.7% and 79% of the observed total clearance, respectively. These data clearly demonstrated that ML00960317 is eliminated mainly through the biliary route in rats potentially involving both sinusoidal uptake and bile canalicular efflux transporters given its low permeability. To further understand the translatability of this finding to humans, we examined biliary CL of ML00960317 using the SCHH model. BEI data obtained in SCHH clearly demonstrated significant biliary excretion of this compound. Interestingly, the biliary CL of ML00960317 was found to be much less than the biliary CL of taurocholate, a high biliary CL compound. However, it was approximately 13% of the biliary CL of digoxin, a low biliary CL compound, indicating some potential for excretion into the bile. Biliary CL is a function of multiple processes, including uptake across the sinusoidal membrane and excretion across the canalicular membrane, therefore, the apparent intrinsic biliary CL would be rate-limited by the slowest step in the process. Although substantial biliary efflux potential for ML00960317 was observed in SCHH, the uptake of ML00960317 appeared to limit the overall biliary CL.

Based on these *in vitro* and *in vivo* hepatobiliary disposition data, we investigated the transporters involved in the hepatic uptake and biliary excretion of ML00960317. The uptake data using single transporter overexpressed HEK cells indicated that the hepatic uptake of ML00960317 is primarily driven by OATP1B1 and OATP1B3 and this was confirmed in human hepatocytes as the uptake of ML00960317 was completely inhibited by rifamycin SV which is known to selectively inhibits OATPs at 20 µM. Subsequently, we quantitatively measured the contribution of OATP1B1 and OATP1B3 to the hepatic uptake of ML00960317 using REF approach. Previously, the REF approach has been

Fig. 2 Analysis of substrate potential of ML00960317 in OATP1B1, OATP1B3, OATP2B1, NTCP, and OAT2-overexpressing cell lines. The uptake of ML00960317 was measured at 37°C in HBSS buffer in OATP1B1 overexpressing HEK cells in the absence (blue bar) and presence of rifamycin SV (20 μM, red bar), and HEK-mock cells (gray) (**a**), in OATP1B3 overexpressing HEK cells in the absence (blue bar) and presence of rifamycin SV (20 μM, red bar), and HEK-mock cells (gray) (**c**), in OATP2B1 overexpressing MDCKII cells (gray) and MDCKII-mock cells (black) (**e**), NTCP overexpressing MDCKII cells (gray) and MDCKII-mock cells (black) (**g**), OAT2 overexpressing MDCKII cells (gray) and MDCKII-mock cells (black) (**i**) for 5 min. The concentration of ML00960317 was 1 μM in OATP1B1 and OATP1B3, and 2 μM in OATP2B1, NTCP, and OAT2 assays. The uptake of [^{3}H]estradiol-17β-glucuronide (0.06 μM), [^{3}H]estrone-3-sulfate (0.5 μM), [^{3}H]TCA (2 μM), and [^{3}H]cyclic guanosine monophosphate (cGMP) (2 μM) was measured in parallel as a positive control substrate of OATP1B1 (**b**) and OATP1B3 (**d**), OATP2B1 (**f**), NTCP (**h**), and OAT2 (**j**), respectively. The gray and black bars indicate the uptake of a positive control substrate in the respective transporter overexpressed cells and mock cells, respectively. The experiment was done in triplicate ($n = 3$). **$**P \leq 0.005$; ***$P < 0.001$, Student's t test
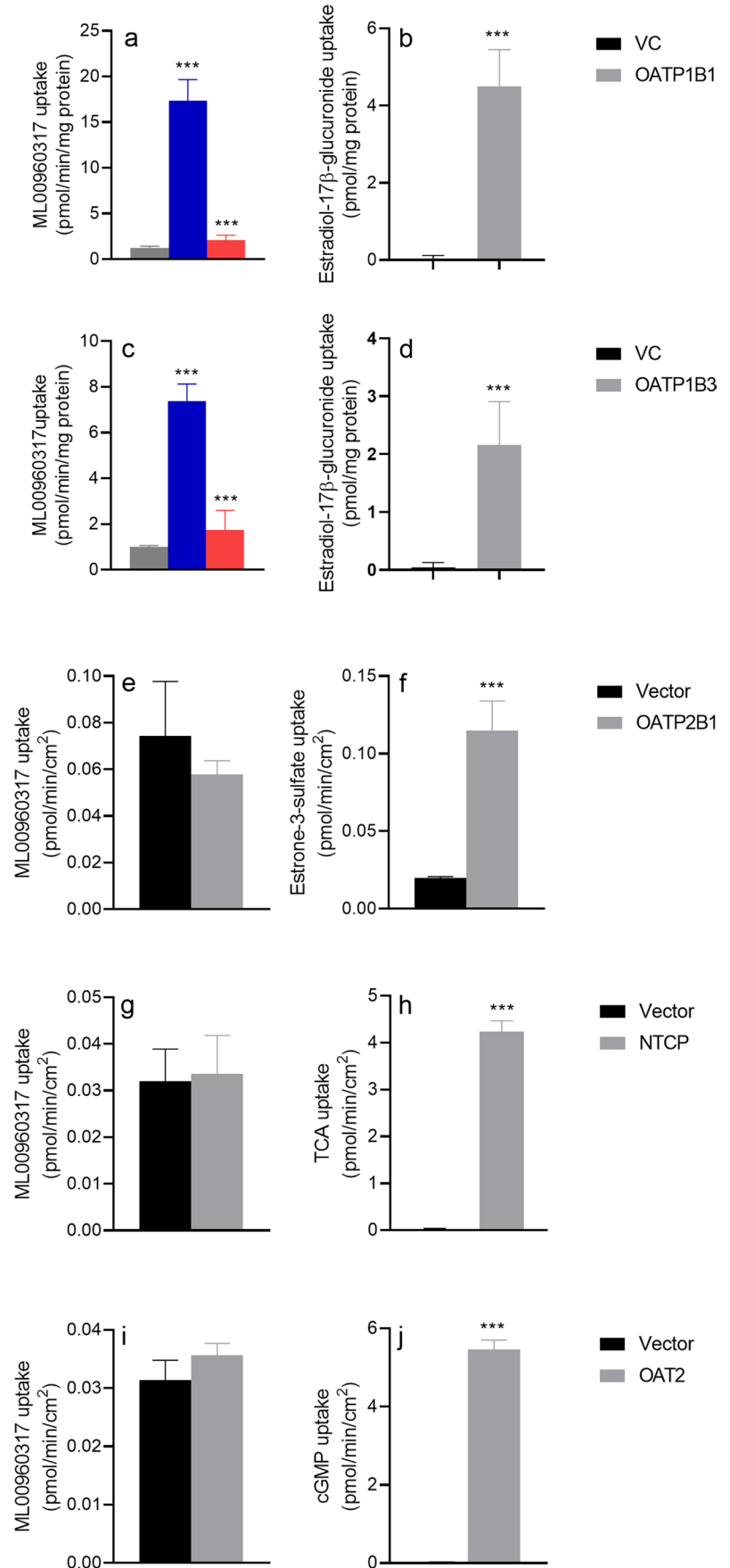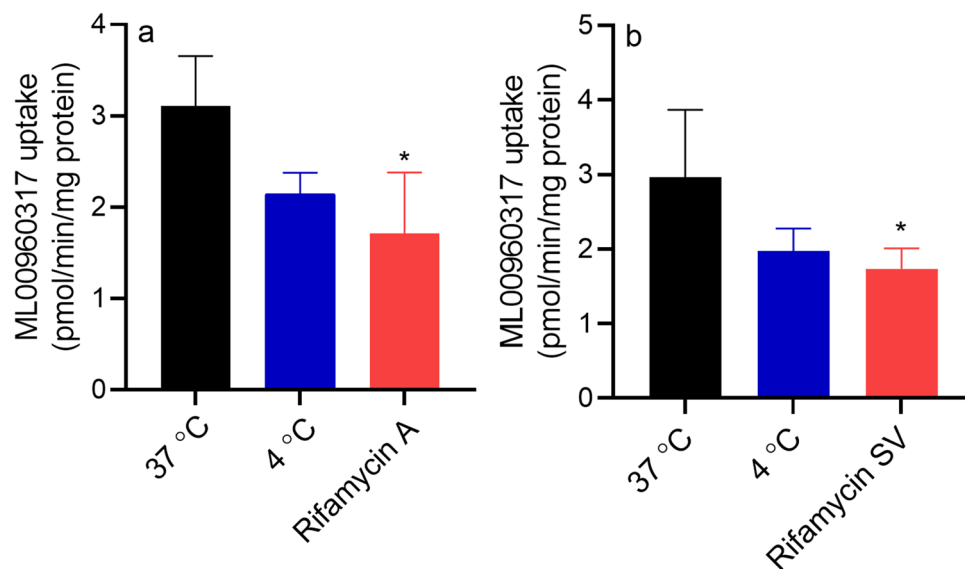
Fig. 3 Assessment of ML00960317 uptake in plated human hepatocytes. The uptake of ML00960317 (1 μM) was measured at 37°C in the absence and presence of rifamycin SV (20 μM) and at 4°C in plated human hepatocytes lot 8339 (**a**) and 8350 (**b**). The black bars indicate the uptake of ML00960317 at 37°C, the blue bars indicate the uptake of ML00960317 at 4°C and the red bars indicate the uptake of ML00960317 at 37°C in the presence of 20 μM rifamycin SV. The data is representative of the two independent experiments performed in each lot of hepatocyte. Each experiment was done in triplicate ($n = 3$). *$P < 0.05$, one-way ANOVA followed by Dunnett's test
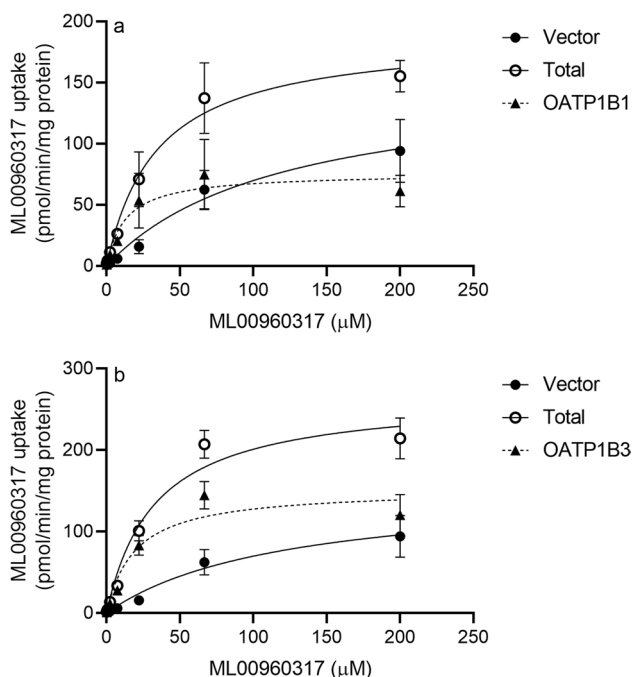
Fig. 4 Measurement of uptake kinetics of ML00960317 in OATP1B1 and OATP1B3 cells. The uptake of ML00960317 was measured in OATP1B1 (**a**) and OATP1B3 (**b**) cells and HEK-mock cells at different concentrations ranging from 0.27 to 200 μM for 5 min in HBSS buffer. The open circles denote the uptake in OATP1B1 or OATP1B3 expressing cells, solid circles denote the uptake in HEK-mock cells, and solid triangles denote the active uptake. The data is representative of the two independent experiments and each experiment was done in triplicate ($n = 3$)

successfully applied to quantitatively determine the contribution of OATPs to the hepatic clearance of many drugs (7, 25, 31). Our data indicated that the combined contribution of OATP1B1 and OATP1B3 to the hepatic uptake of ML00960317 is between 91 and 93% and in that, OATP1B1 appears to be the major contributor compared to OATP1B3 (f_t of 0.6 for OATP1B1 *versus* f_t of 0.31 for OATP1B3). We also determined contribution of OATP1B1 and OATP1B3 to the uptake clearance of atorvastatin (known OATP substrate), as a positive control. The combined contribution of OATP1B1 and OATP1B3 to atorvastatin uptake clearance was found to be between 61 and 85% whereas the fraction transported (f_t) by OATP1B1 and OATP1B3 was between 0.38–0.52 and 0.23–0.33, respectively. This data is consistent with the data reported by Kunze *et al.* in which total contribution of OATP1B1 and OATP1B3 was 63% and fraction transported by OATP1B1 was 0.5. However, in the present study, the fraction transported by OATP1B3 appears to be relatively higher than that found in the study by Kunze *et al.* ($f_t = 0.13$) (25). This might be attributed to the differences in the expression and function of OATP1B3 in hepatocyte lots. Indeed, the protein expression of OATP1B3 relative to OATP1B1 in hepatocyte lots used in this study (4.5-fold lower) was much higher than the one in the hepatocytes used in the study by Kunze *et al.* (46-fold lower). Interestingly, in the present study, a noticeable difference was found in OATP1B1 contribution to atorvastatin clearance between lot 8350 (61%) and the lot 8339 (85%). The potential reason for

Fig. 5 Substrate analysis of ML00960317 in MDR1, BCRP, and MRP2-expressing membrane vesicles. The uptake of ML00960317 was measured at in MDR1 (**a**), BCRP (**b**), and MRP2 (**c**), expressing membrane vesicles at 0.18, 1.83, and 9.15 μM for 10 min in the presence of AMP (black bars) and ATP (gray bars). The experiment was done in triplicate ($n = 3$). ***$P < 0.001$, Student's t test
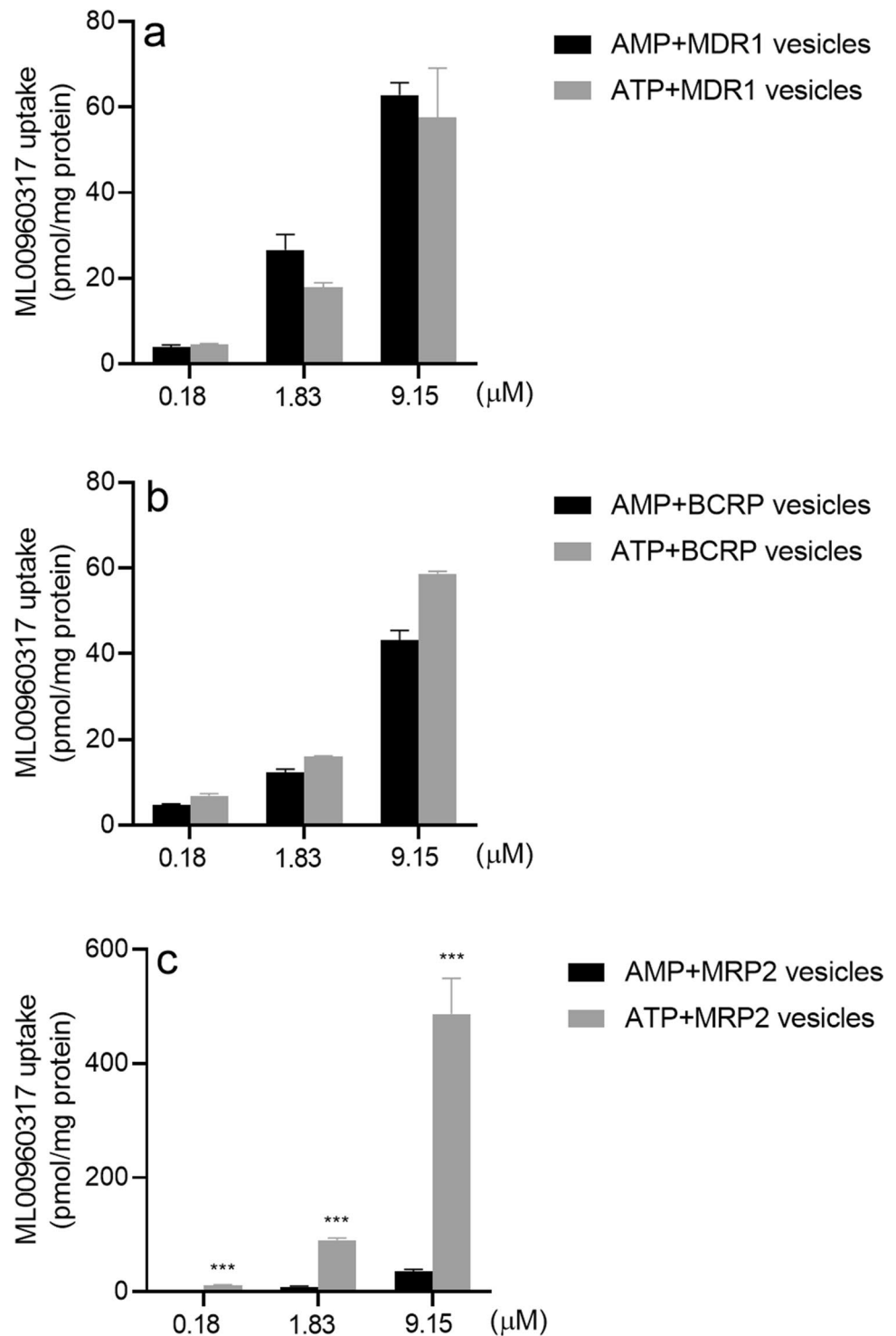
this difference may be due to the higher expression (5-fold) of NTCP in 8350 lot compared to 8339 lot. NTCP is known to transport atorvastatin (32, 33).

Recently, reduced-folate carrier (RFC, *SLC19A1*) (6, 34), thymic stromal cotransporter (*SLC46A2*) (35), and volume regulated chloride channel complex (*LRRC8:C*) (36) have been shown to transport the endogenous CDN (2′3′-cGAMP). Therefore, to investigate the potential role of these transporters in the hepatic uptake of ML00960317, we decided to measure their protein levels in human hepatocyte lots 8339 and 8350. However, we did not find the expression of *SLC19A1* to be detectable in these hepatocyte lots. We did not measure the protein abundance of *SLC46A2* and *LRRC8A:C* due to lack of
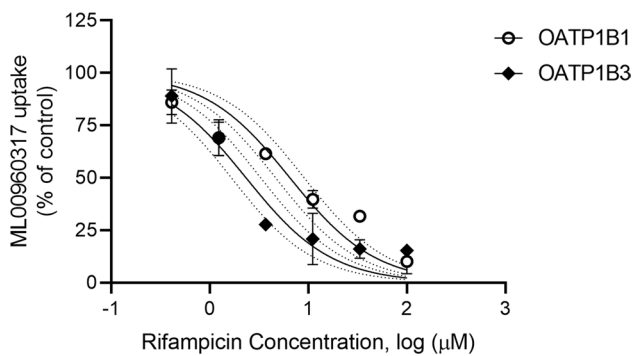
Fig. 6 Inhibition of OATP1B1 and OATP1B3-mediated ML00960317 uptake by rifampicin. HEK-mock and HEK cells overexpressing OATP1B1 and OATP1B3 were pre-incubated with rifampicin at different concentrations between 0.4 and 100 μM for 30 min and then co-incubated with different concentrations of rifampicin and ML00960317 for 5 min. The uptake of ML00960317 in HEK-mock cells was subtracted from its uptake in OATP1B1 and OATP1B3 overexpressing HEK cells. The data is shown as the percent of DMSO control. The data is representative of the two independent experiments and each experiment was done in triplicate ($n = 3$)

validated surrogate peptides for LC-MS analysis. Nonetheless, the role of *SLC46A2* and *LRRC8A:C* transporters in the hepatic uptake of ML00960317 is less likely as in the present study, the hepatocyte uptake data using 20 μM rifamycin SV (selective OATP inhibitor) indicated involvement of only OATPs. Taken together, these data revealed that the uptake of ML00960317 is solely mediated by OATP1B1 and OATP1B3 in the liver.

To delineate the transporters involved in the biliary efflux of ML00960317, the transport of this compound was tested in membrane vesicles expressing MDR1, BCRP, and MRP2 which are major efflux transporters for drugs at the bile canalicular membrane. We did not examine BSEP because it is not known to transport drugs due to its high specificity to bile salts (37). BSEP has been shown to transport pravastatin (38) but its contribution to the *in vivo* CL of pravastatin is unknown. The membrane vesicle data clearly demonstrated ML00960317 as a substrate of MPR2 but not MDR1 and BCRP. Taken together, all the transporter data presented in this study clearly demonstrated the two key steps in the hepatobiliary disposition of ML00960317 — OATP1B-mediated uptake at the sinusoidal membrane and MRP2-mediated efflux at the basolateral membrane. These findings are consistent with the recent report by Jiang R *et al.* in which OATP1B1, OATP1B3, and MRP2 have been shown to be involved in the hepatic disposition of macrocycle-bridged dinucleotide, E7766 (7). Nonetheless, we observed a significant difference in the present study and the study by Jiang *et al*. in terms of OATP1B1 and OATP1B3 contribution. In the study by Jiang R. *et al*., OATP1B3 appeared to be a major contributor ($f_t = 0.93$) to the uptake CL of E7766 while in

the present study, both OATP1B1 and OATP1B3 (although to lesser extent) appear to contribute to the uptake CL of ML00960317. Due to significant contribution of OATP1B1, ML00960317 may be impacted by OATP1B1 polymorphism especially in OATP1B1 521C variant homozygous population. Additionally, there is also a potential victim DDI risk *in vivo* for ML00960317 in the presence of OATP1B perpetrators as demonstrated by rifampicin in the present study (Fig. 6).

In summary, the data presented in this study highlighted the key role of OATP1B and MRP2 transporters in the hepatobiliary disposition of synthetic CDN STING agonist, ML00960317. These transport processes might act as rate-determining steps in hepatic clearance of such drugs and therefore present DDI risk with OATP1B and MRP2 perpetrators. Thus, the present study provides mechanistic insights into hepatic disposition for future development of synthetic CDN STING agonists as a promising anti-cancer strategy.

Declarations

References

1. Finn OJ. Immuno-oncology: understanding the function and dysfunction of the immune system in cancer. Ann Oncol. 2012;23 Suppl 8:viii6-9. https://doi.org/10.1093/annonc/mds256.

2. Wang H, Hu S, Chen X, Shi H, Chen C, Sun L, *et al*. cGAS is essential for the antitumor effect of immune checkpoint blockade. Proc Natl Acad Sci USA. 2017;114(7):1637–42. https://doi.org/10.1073/pnas.1621363114.

3. Corrales L, Glickman LH, McWhirter SM, Kanne DB, Sivick KE, Katibah GE, et al. Direct activation of STING in the tumor microenvironment leads to potent and systemic tumor regression and immunity. Cell Rep. 2015;11(7):1018–30. https://doi.org/10.1016/j.celrep.2015.04.031.

4. Apelbaum A, Yarden G, Warszawski S, Harari D, Schreiber G. Type I interferons induce apoptosis by balancing cFLIP and caspase-8 independent of death ligands. Mol Cell Biol. 2013;33(4):800–14. https://doi.org/10.1128/MCB.01430-12.

5. Vyskocil S, Cardin D, Ciavarri J, Conlon J, Cullis C, England D, et al. Identification of novel carbocyclic pyrimidine cyclic dinucleotide STING agonists for antitumor immunotherapy using systemic intravenous route. J Med Chem. 2021;64(10):6902–23. https://doi.org/10.1021/acs.jmedchem.1c00374.

6. Luteijn RD, Zaver SA, Gowen BG, Wyman SK, Garelis NE, Onia L, et al. SLC19A1 transports immunoreactive cyclic dinucleotides. Nature. 2019;573(7774):434–8. https://doi.org/10.1038/s41586-019-1553-0.

7. Jiang R, Hart A, Burgess L, Kim DS, Lai WG, Dixit V. Prediction of transporter-mediated drug-drug interactions and phenotyping of hepatobiliary transporters involved in the clearance of E7766, a novel macrocycle-bridged dinucleotide. Drug Metab Dispos. 2021;49(3):265–75. https://doi.org/10.1124/dmd.120.000125.

8. Varma MV, Steyn SJ, Allerton C, El-Kattan AF. Predicting clearance mechanism in drug discovery: Extended Clearance Classification System (ECCS). Pharm Res. 2015;32(12):3785–802. https://doi.org/10.1007/s11095-015-1749-4.

9. Maeda K, Ikeda Y, Fujita T, Yoshida K, Azuma Y, Haruyama Y, et al. Identification of the rate-determining process in the hepatic clearance of atorvastatin in a clinical cassette microdosing study. Clin Pharmacol Ther. 2011;90(4):575–81. https://doi.org/10.1038/clpt.2011.142.

10. Watanabe T, Kusuhara H, Maeda K, Kanamaru H, Saito Y, Hu Z, et al. Investigation of the rate-determining process in the hepatic elimination of HMG-CoA reductase inhibitors in rats and humans. Drug Metab Dispos. 2010;38(2):215–22. https://doi.org/10.1124/dmd.109.030254.

11. Kimoto E, Mathialagan S, Tylaska L, Niosi M, Lin J, Carlo AA, et al. Organic anion transporter 2-mediated hepatic uptake contributes to the clearance of high-permeability-low-molecular-weight acid and zwitterion drugs: evaluation using 25 drugs. J Pharmacol Exp Ther. 2018;367(2):322–34. https://doi.org/10.1124/jpet.118.252049.

12. Fan PW, Chen JZ, Allan Jaochico M, La H, Liu N, Mulder T, et al. Rate-determining and rate-limiting steps in the clearance and excretion of a potent and selective p21-activated kinase inhibitor: a case study of rapid hepatic uptake and slow elimination in rat. Drug Metab Lett. 2016;10(2):91–100. https://doi.org/10.2174/1872312810666160411144358.

13. Kong LL, Shen GL, Wang ZY, Zhuang XM, Xiao WB, Yuan M, et al. Inhibition of P-glycoprotein and multidrug resistance-associated protein 2 regulates the hepatobiliary excretion and plasma exposure of thienorphine and its glucuronide conjugate. Front Pharmacol. 2016;7:242. https://doi.org/10.3389/fphar.2016.00242.

14. Futatsugi A, Toshimoto K, Yoshikado T, Sugiyama Y, Kato Y. Evaluation of alteration in hepatic and intestinal bcrp function in vivo from ABCG2 c.421C>A polymorphism based on PBPK analysis of rosuvastatin. Drug Metab Dispos. 2018;46(5):749–57. https://doi.org/10.1124/dmd.117.078816.

15. Tian X, Zamek-Gliszczynski MJ, Li J, Bridges AS, Nezasa K, Patel NJ, et al. Multidrug resistance-associated protein 2 is primarily responsible for the biliary excretion of fexofenadine in mice. Drug Metab Dispos. 2008;36(1):61–4. https://doi.org/10.1124/dmd.107.017319.

16. Yoshikado T, Maeda K, Furihata S, Terashima H, Nakayama T, Ishigame K, et al. A clinical cassette dosing study for evaluating the contribution of hepatic OATPs and CYP3A to drug-drug interactions. Pharm Res. 2017;34(8):1570–83. https://doi.org/10.1007/s11095-017-2168-5.

17. Kalliokoski A, Neuvonen PJ, Niemi M. SLCO1B1 polymorphism and oral antidiabetic drugs. Basic Clin Pharmacol Toxicol. 2010;107(4):775–81. https://doi.org/10.1111/j.1742-7843.2010.00581.x.

18. Niemi M, Backman JT, Kajosaari LI, Leathart JB, Neuvonen M, Daly AK, et al. Polymorphic organic anion transporting polypeptide 1B1 is a major determinant of repaglinide pharmacokinetics. Clin Pharmacol Ther. 2005;77(6):468–78. https://doi.org/10.1016/j.clpt.2005.01.018.

19. He YJ, Zhang W, Chen Y, Guo D, Tu JH, Xu LY, et al. Rifampicin alters atorvastatin plasma concentration on the basis of SLCO1B1 521T>C polymorphism. Clin Chim Acta. 2009;405(1-2):49–52. https://doi.org/10.1016/j.cca.2009.04.003.

20. Pasanen MK, Fredrikson H, Neuvonen PJ, Niemi M. Different effects of SLCO1B1 polymorphism on the pharmacokinetics of atorvastatin and rosuvastatin. Clin Pharmacol Ther. 2007;82(6):726–33. https://doi.org/10.1038/sj.clpt.6100220.

21. Sandoval P, Chuang BC, Cohen L, Yoneyama T, Pusalkar S, Yucha RW, et al. Sinusoidal uptake determines the hepatic clearance of pevonedistat (TAK-924) as explained by extended clearance model. Drug Metab Dispos. 2022. https://doi.org/10.1124/dmd.122.000836.

22. Chothe PP, Pemberton R, Hariparsad N. Function and expression of bile salt export pump in suspension human hepatocytes. Drug Metab Dispos. 2021;49(4):314–21. https://doi.org/10.1124/dmd.120.000057.

23. Khatri R, Fallon JK, Rementer RJB, Kulick NT, Lee CR, Smith PC. Targeted quantitative proteomic analysis of drug metabolizing enzymes and transporters by nano LC-MS/MS in the sandwich cultured human hepatocyte model. J Pharmacol Toxicol Methods. 2019;98:106590. https://doi.org/10.1016/j.vascn.2019.106590.

24. Kumar AR, Prasad B, Bhatt DK, Mathialagan S, Varma MVS, Unadkat JD. In vivo-to-in vitro extrapolation of transporter-mediated renal clearance: relative expression factor versus relative activity factor approach. Drug Metab Dispos. 2020;49(6):470–8. https://doi.org/10.1124/dmd.121.000367.

25. Kunze A, Huwyler J, Camenisch G, Poller B. Prediction of organic anion-transporting polypeptide 1B1- and 1B3-mediated hepatic uptake of statins based on transporter protein expression and activity data. Drug Metab Dispos. 2014;42(9):1514–21. https://doi.org/10.1124/dmd.114.058412.

26. Liu X, Chism JP, LeCluyse EL, Brouwer KR, Brouwer KL. Correlation of biliary excretion in sandwich-cultured rat hepatocytes and in vivo in rats. Drug Metab Dispos. 1999;27(6):637–44.

27. Wilson ZE, Rostami-Hodjegan A, Burn JL, Tooley A, Boyle J, Ellis SW, et al. Inter-individual variability in levels of human microsomal protein and hepatocellularity per gram of liver. Br J Clin Pharmacol. 2003;56(4):433–40. https://doi.org/10.1046/j.1365-2125.2003.01881.x.

28. Davies B, Morris T. Physiological parameters in laboratory animals and humans. Pharm Res. 1993;10(7):1093–5. https://doi.org/10.1023/a:1018943613122.

29. Sandker GW, Weert B, Olinga P, Wolters H, Slooff MJ, Meijer DK, et al. Characterization of transport in isolated human hepatocytes. A study with the bile acid taurocholic acid, the uncharged ouabain and the organic cations vecuronium and rocuronium. Biochem Pharmacol. 1994;47(12):2193–200. https://doi.org/10.1016/0006-2952(94)90255-0.

30. Lu Y, Slizgi JR, Brouwer KR, Claire RL, Freeman KM, Pan M, et al. Hepatocellular disposition and transporter interactions with tolvaptan and metabolites in sandwich-cultured human hepatocytes. Drug Metab Dispos. 2016;44(6). https://doi.org/10.1124/dmd.115.067629.

31. Kumar V, Yin M, Ishida K, Salphati L, Hop C, Rowbottom C, et al. Prediction of transporter-mediated rosuvastatin hepatic uptake clearance and drug interaction in humans using proteomics-informed REF approach. Drug Metab Dispos. 2021;49(2):159–68. https://doi.org/10.1124/dmd.120.000204.

32. Vildhede A, Karlgren M, Svedberg EK, Wisniewski JR, Lai Y, Noren A, et al. Hepatic uptake of atorvastatin: influence of variability in transporter expression on uptake clearance and drug-drug interactions. Drug Metab Dispos. 2014;42(7):1210–8. https://doi.org/10.1124/dmd.113.056309.

33. Wang Y, Wilkerson M, Li J, Zhang W, Owens A, Wright S, et al. Assessment of statin interactions with the human NTCP transporter using a novel fluorescence assay. Int J Toxicol. 2020;39(6):518–29. https://doi.org/10.1177/1091581820953066.

34. Ritchie C, Cordova AF, Hess GT, Bassik MC, Li L. SLC19A1 Is an importer of the immunotransmitter cGAMP. Mol Cell. 2019;75(2):372–81 e5. https://doi.org/10.1016/j.molcel.2019.05.006.

35. Cordova AF, Ritchie C, Bohnert V, Li L. Human SLC46A2 is the dominant cGAMP importer in extracellular cGAMP-sensing macrophages and monocytes. ACS Cent Sci. 2021;7(6):1073–88. https://doi.org/10.1021/acscentsci.1c00440.

36. Lahey LJ, Mardjuki RE, Wen X, Hess GT, Ritchie C, Carozza JA, et al. LRRC8A:C/E heteromeric channels are ubiquitous transporters of cGAMP. Mol Cell. 2020;80(4):578–91 e5. https://doi.org/10.1016/j.molcel.2020.10.021.

37. Kubitz R, Droge C, Stindt J, Weissenberger K, Haussinger D. The bile salt export pump (BSEP) in health and disease. Clin Res Hepatol Gastroenterol. 2012;36(6):536–53. https://doi.org/10.1016/j.clinre.2012.06.006.

38. Hirano M, Maeda K, Hayashi H, Kusuhara H, Sugiyama Y. Bile salt export pump (BSEP/ABCB11) can transport a nonbile acid substrate, pravastatin. J Pharmacol Exp Ther. 2005;314(2):876–82. https://doi.org/10.1124/jpet.105.084830.

Publisher's Note Springer Nature remains neutral with regard to jurisdictional claims in published maps and institutional affiliations.